ETEAPOT EDM, Benchmark-III: Updated Results: Dispersion, Longitudinal Dynamics and Synchrotron Oscillations

J. D. Talman and R. M. Talman

November 16, 2019

Abstract

In this chapter ETEAPOT is used to study longitudinal motion in the three benchmark lattices documented in previous chapters. These lattices have field indices $m = -1$, $m \approx 0$, and $m = 1$. Most of the results this time are presented only for one or the other of the $m = -1, 0, 1$ cases, since most longitudinal quantities are very nearly the same for all three once their vertical tunes have all been adjusted to Q_y=0.2.

The three benchmark lattices were chosen to be especially simple, with optics dominated by the (weak focusing) electric bend elements. Unfortunately the resulting quite large dispersion complicates the longitudinal dynamics.

Evaluations of dispersion, synchroton oscillations, and physical acceptances are compared with analytical calculations and with calculations using the same linearized transfer matrix formalism described in the earlier benchmark reports[1][2]. Agreement is excellent for the lattice dispersion, but ETEAPOT finds small-amplitude synchrotron tunes to be 20% smaller than the analytic approximation predicts. This may be due to the neglect (in the analytic calculation) of the quadrupoles used to adjust the tunes to standard values. It may also be due to hypersensitivity resulting from the high lattice dispersion.

Accepting the ETEAPOT simulation results as valid, a detailed study of longitudinal motion is completed. There is excellent agreement with the expectations for Q_s to vary proportional to the square root of RF voltage and for the bunch length to vary inversely to the square root of RF voltage. Stability for at least one million turns is demonstrated for sufficiently small synchrotron oscillation amplitude; any spurious growth in the simulation has a growth lifetime of at least three million turns. Both qualitatively and quantitatively synchrotron oscillations seem to behave in electric lattices much the way they do in magnetic lattices.

1   Subtle features of longitudinal motion in all-electric rings

Evolution through thick elements in ETEAPOT (as in TEAPOT) is analytically exact. In ETEAPOT this includes also spin evolution. This exact treatment is only possible for certain electric or magnetic force fields—uniform magnetic fields for magnets, inverse square law (a.k.a. "Kepler") for electric fields. In neither case are the as-built, realistic accelerator force fields nearly this ideally uniform. In ETEAPOT (as in TEAPOT) the deviations from ideal are represented by thin (and hence symplectic) elements. This approach proved valid in TEAPOT, for both electrons and positrons, for example in calculating dynamic apertures of SSC, LHC, CESR, etc. And we regard the approach to be essential for faithful spin tracking.

The beauty of point sources is that the force fields of point sources are central. As a result their 3D orbits are, in fact, restricted to two dimensional planes. For non-relativistic Kepler planetary orbits the orbits are perfect ellipses. The protons in proposed EDM storage rings are sufficiently relativistic that

the orbits are not exactly elliptical, but the deviations from ideal ellipse show up only in "advances of perihelion" of the order of 45 degrees per revolution. Through short bend elements the orbits look pretty much like ellipses—in fact they even look pretty much like circles. The exact analytic expressions can be represented by "ellipses" with "varying constant" major axis and eccentricity. This evolution is well known and is known to be valid as long as general relativity effects remains negligible.

The orientation of a (relativistic) Kepler orbit can be specified by the orientation of its major (or minor) axis, and the particle position can be specified by a very simple analytic formula (first obtained by Newton) depending only on an angle $\theta - \theta_0$ which is the angle between the particle angle θ and the perihelion angle θ_0.

The description of accelerator orbits as (relativistic) Kepler orbits has one inelegant feature; namely, on the central design orbit, the orbit is circular and there is no unambiguous perihelion angle. In this sense, *the central orbit is singular.* In principle this should not be a problem, as the code can define the perihelion angles arbitrarily for each particle and then keep track of their evolutions. This includes the requirement, when the orbit switches from oblate to prolate, for θ_0 to change discontinuously. *This is easier said than done.*
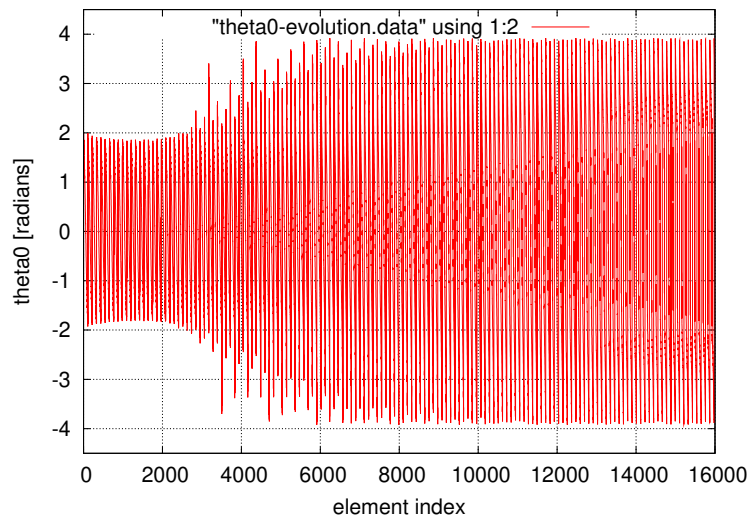

Figure 1: Evolution of perihelion angle θ_0 for 100 turns of a single particle in the `E_BM_M1.0.RF` proton EDM ring. as discussed in the text, erratic behavior starting at element index 3500 or so is due to a bug (now removed) in distinguishing between angles of perihelion and apheliom.

Figure (1) shows the evolution of θ_0 for a particle being tracked through 16,000 elements (which is about 100 revolutions) around the `E_BM_M1.0.RF` ring. It can be seen that the evolution of θ_0 is somewhat erratic. For the first 3000 or so elements θ_0 oscillates between two extremes. One would prefer a "constant" to be more nearly constant than this, but the behaviour is not unexpected, as the orbit switches periodically from oblate to prolate (relative to the selected perihelion or aphelion angle).

Because the particle evolution through bend elements depends only on $\theta - \theta_0$, this alternation has no effect on the calculated transverse orbit evolution. But the longitudinal effect of the alternation was not handled correctly in preliminary ETEAPOT time of flight calculations. This bug caused the longitudinal evolution to be treated incorrectly.

One effect of this error was to destroy reflection symmetry in the horizontal (*ct*-axis) phase space plot). Fixing the bug restored this symmetry. (See Figure 3.) As it happens, the longitudinal stability seemed to be not very much disturbed, though fixing the bug altered the synchrotron tune by about 30 percent.

There is a further, and more disturbing, feature of Figure 1. It is the erratic variation of θ_0 which is first visible on turn 3500 or so. Zooming in on this region one sees that, when the orbit is quite accurately

circular, the perihelion can jitter back and forth several times before settling down to steady alternation. This seems to have been the source of the (non-Liouvillian) beam growth, referred to as resonant blow-up in a preliminary report.

As described so far ETEAPOT can be described as "geometric". From an aesthetic point of view this is quite elegant. One sees however, that, as mentioned above, the fact that the design orbit is singular, essentially guarantees the existence of occasional jittering between oblate and prolate parameterizations. Though the code should, in principle, be able to handle this jittering correctly, the initial code certainly did not.

The current ETEAPOT code avoids this jittering by introducing a truncated Taylor series representation of the orbit. This alternate approach is quite conventional from an accelerator physics standpoint. Since this code is fully described in the updated `ETEAPOT-expanded.pdf` documentation it will not be discussed in detail here. With this code incorporated, transverse evolution through bends of every particle is now worked out in two different, and almost completely independent, ways. To avoid the erratic θ_0 determination, only the truncated Taylor series approach is used for time of flight calculations. (Technically this requires the time of flight to be evaluated using a power series. This is less elegant than the analytically exact integral determination, but the series converges rapidly enough to be essentially exact. This circumvents the erratic geometric behavior of near circular orbits.)

There has been a factor of two computation slow down resulting from the dual calculations that have been described. We have chosen to accept this performance hit for the time being. The performance can be recovered either by stripping the code or, better, parallel computation.

The last figure of this section compares transverse evolution as calculated by the "geometric" or "Muñoz" approach and by the (more nearly conventional accelerator) truncated Taylor series approach. Transverse evolution through the same 16,000 elements as calculated the two independent ways is com-
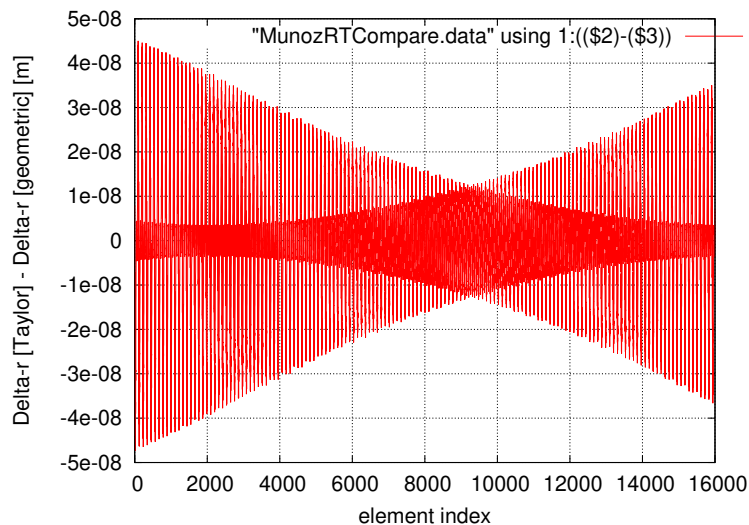

Figure 2: Deviation between evolutions of transverse coordinate x as calculated by (accelerator-style) Taylor series formulation and the (geometric, or Muñoz, or astronomical) formulation.

pared in Figure 2. The difference between radial position calculations never exceeds 4.5×10^{-8} m and, on the average, the deviation is less than 10^{-9} m. As well as providing increased confidence in the tracking, this figure also explains why the (now-repaired) bug affected longitudinal evolution without affecting transverse evolution.

3

2 Parameters of Benchmark Lattices

Transverse parameters for the benchmark lattices are given in Table 1; these have been copied from pevious reports. Longitudinal parameters of the same lattices are given in Table 2; the entries are explained in later sections.

Table 1: Transverse parameters of benchmark all-electric EDM lattices copied from benchmark comparisons I and II.

file name	variable name	unit	E_BM_M1.0.RF.sxf	E_BM_Z.RF.sxf	E_BM_P1.0.RF.sxf
cells/arc	NCellPerArc		20	20	20
bend radius	r0	m	40.0	40.0	40.0
half drift length	Ldh	m	1.0	1.0	1.0
half bend per cell	Thetah	r	0.078539816	0.078539816	0.078539816
half bend length	Leh	m	3.141592	3.141592	3.141592
circumference	circum	m	331.327	331.327	331.327
inverse focal length	q	1/m	-0.002019	-0.00005960	0.0019075
field index	m		-1.0	1.0e-10	1.0
horizontal beta	betax	m	35.9237	36.1018	36.1910
vertical beta	betay	m	264.182	263.620	262.237
horizontal tune	Qx		1.4605	1.4578	1.4588
vertical tune	Qy		0.20024	0.20004	0.20047

Table 2: Longitudinal parameters (in MAD/UAL units) for the E_BM_M1.0.RF.sxf benchmark all-electric EDM lattice. Most of these quantities are very nearly the same for the E_BM_Z.RF.sxf and E_BM_P1.0.RF.sxf. This can be seen, for example, in Figure 4. Uncertainties in the analytic values are discussed in the text.

file name	symbol	unit	analytic	MAPLE	ETEAPOT
Rev. period	$T_{\mathrm{rev}}(\gamma_0)$	μs	1.846972	1.846972	1.846972
	$dT_{\mathrm{rev}}/d\gamma\|_{\gamma_0}$	μs	2.49127		
RF frequency	f_{RF}	MHz	$0.541426\,h_{\mathrm{RF}}$		$0.541426\,h_{\mathrm{RF}}$
harmonic number	h_{RF}		100		100
RF peak voltage§	$\hat{V}_{\mathrm{RF}}$	kV	1.0		1.0
RF phase lag¶	ϕ_{RF}	radian	0.5		0.5
dispersion	D_{UAL}	m	66.9, Eq.(12)	$24.8 \times 2.74 = 67.9$	66.9
slip factor	η_{RF}		$\approx$ -0.92, Eq.(18)		
synch. tune (lo)	$Q_s(10^{-6})$		$\approx$ 0.0061, Eq.(19)		0.0049, Fig.7
synch. tune (hi)	$Q_s(2 \times 10^{-5})$				0.0048, Fig.12
ang. accept. (short)					$\pm$0.0004, Fig.11
ang. accept. (long)					$< \pm$0.0002, Fig.13

§RF voltage drop in GV,   ¶RF phase shift in units of 2π

3 Comparison of Fractional Momentum and Energy Offset Parameters

Different communities prefer different definitions of the fractional momentum or energy offset. Wollnik (Section 4.1.1.2) defines the "rigidity offset" Δ of an off-energy particle by

$$r = r_0(1 + \Delta), \quad \text{or} \quad \delta_{\text{Wollnik}} \equiv \Delta = \frac{r - r_0}{r_0}, \tag{1}$$

where r_0 is the nominal bend radius, and r is the radius of a concentric circular orbit followed by the off-momentum particle. This is the fractional offset coordinate applicable to the linearized transfer matrix benchmark comparison results in this report. For "sector bends" in which all orbits enter and exit more or less normal to the edges of the bend element there is hardly any need to distinguish between radial offsets outside and inside bend elements.

ETEAPOT (like MAD) defines a fractional energy offset,

$$\delta_{\text{UAL}} \equiv \frac{\mathcal{E}^O - \mathcal{E}_0{}^O}{p_0^O c}. \tag{2}$$

The superscript O is attached to $\mathcal{E}^O$ and p^O here to specify that these quantities are restricted to regions "outside" bend regions; i.e. where the potential energy vanishes. (For $\mathcal{E}$ this notation is redundant since $\mathcal{E}$ is preserved except in RF cavities. As it happens it is also redundant for p_0 since, by definition, the potential energy vanishes everywhere on the design orbit.)

- It is shown in the ETEAPOT manual that the Wollnik Δ parameter is related to the MAD/UAL momentum deviation factor δ_{UAL} by

$$\Delta = \left(1 + \frac{1}{\gamma_0^2}\right) \frac{1}{\beta_0} \delta_{\text{UAL}} \quad \left(= 2.744\, \delta_{\text{UAL}} \quad \text{for the proton EDM experiment.}\right) \tag{3}$$

- A notation commonly employed in the electron and proton accelerator worlds (with jargon "delta p over p") is

$$\delta_p \equiv \frac{p^O - p_0}{p_0}. \tag{4}$$

(We intentionally refrain from introducing a momentum-inside variable δ_{p^I}; defined in terms of this variable the dispersion $D_{\delta_{p^I}}$ would be singular for field index $m = 0$.) Relations among fractional *outside* momentum or energy coordinates, since they are unaffected by potential energy, can be obtained using standard (for magnetic lattices) kinematic formulas, starting from

$$\mathcal{E}^2 = p^2 c^2 + m_p^2 c^4. \tag{5}$$

For example,

$$\frac{dp}{p_0} = \frac{1}{\beta_0} \frac{d\mathcal{E}^O}{p_0 c}, \quad \text{or} \quad \delta_p = \frac{1}{\beta_0} \delta_{\text{UAL}}. \tag{6}$$

To obtain δ_p (also known as "delta p over p") from δ_{UAL} one must therefore divide δ_{UAL} by 0.6.

- Should one want the absolute change in γ corresponding to δ_{UAL} one has to multiply δ_{UAL} by $p_0 c/(m_p c^2) = 0.7/0.938 = 0.746$. This relation can also be expressed as $d\gamma = \beta_0 \gamma_0 \delta_{\text{UAL}}$.

Having established the principle behind the O-superscript notation, from here on quantities without superscripts are to be interpreted as *outside* quantities. This simplifies the discussion of synchrotron oscillations where it is assumed that the bend field electric potential vanishes throughout RF cavities.

4 Analytic Estimates of Longitudinal Parameters

This section discusses the analytical treatment used to estimate parameters for checking the numerical ETEAPOT results. It is the only section in which it is necessary to deal with the confusing subject of kinematic quantities in the interior of bend elements. The (weak) quadrupoles present in the lattice to trim the tunes are neglected for this treatment. This causes an uncontrolled, but hopefully small, uncertainty in the comparison values.

4.1 Qualitative Discussion of Dispersion

For circular orbits in an electric bend element with radial electric field $-E_0$, the radius of the central orbit is given by

$$r_0 = \frac{m_p c^2/e}{E_0}\, \gamma_0 \beta_0^2. \tag{7}$$

For field index m the radius of curvature of an off-momentum circular orbit is given by

$$r = r_0 \left(\frac{\gamma_0^2 - 1}{\gamma_0}\, \frac{\gamma^I}{\gamma^{I\,2} - 1} \right)^{1/m}, \tag{8}$$

where γ_0 is the value on the central orbit. This relationship is singular for field index $m = 0$ (which is also known as the "cylindrical" case because the electrodes giving this radial dependence are cylindrical). $m = 0$ is also the unique case in which the dependence of electric potential on radius r is logarithmic and cannot be expressed by a power law.

For values of m near 1 the orbit velocities of off-energy circular orbits within bend elements are approximately independent of r. This causes the time of flight of off-energy closed orbits through arcs (which are perfect circles) to be dominated by the arc length, which is the bend angle multiplied by r. Since the speed depends only weakly on momentum this is "above transition" behavior. On the other hand, off-energy closed orbit path lengths through drifts are independent of δ_{UAL}, which causes time of flight of off-energy closed orbits through drifts to be dominated by the particle speed; this is "below transition" behavior. Assuming the drift lengths are fairly short, the net behavior is "above-transition" like.

For negative m values the radius of the off-energy closed orbit inreases with increasing energy offset. The dispersion D is therefore positive for $m < 0$; furthermore the magnitude $|D|$ *increases* as m approaches zero. For positive m values (such as the $m = 1$ "spherical case") the radius of off-energy closed orbits decrease with increasing energy offset. The dispersion D is therefore negative for $m > 0$; but the magnitude $|D|$ again *increases* as m approaches zero.

Realistic lattices also have quadrupoles which affect the dispersion. But, since the quadrupoles are very weak in the three benchmark lattices, their influence on lattice dispersion can be expected to be not very important. (For the minimized-dispersion, strong horizontal focusing, combined function lattices to be recommended as a response to results in the present report, this will no longer be even approximately valid.)

Combining all these statements, the dispersion function D has to have a singularity in the vicinity of $m = 0$. It is the longitudinal dynamics (rather than the transverse) that is sensitive to lattice dispersion. To make them as simple as possible, the m-values of the three benchmark lattices were chosen close to zero. Inadvertently this choice has caused the longitudinal dynamics of the benchmark lattices to be hyper-sensitive.

An example of this hypersensitivity comes about in comparing computer simulation and analytic results. The analytic results depend on the dispersion. But the dispersion is not used, and is not available, during particle tracking. This makes it a priori unkown what RF phase will give stable longitudinal motion in simulation. We resolve this ambiguity by trying two RF phases differing by π and choosing the phase that gives stable motion.

Another subtle complication of operation near $m = 0$ comes about because a particle having positive velocity offset outside bends can have either positive or negative velocity offset inside bends, depending

on the sign of m. This dependence is transparent to the computer simulation but complicates the analytic calculation of the "slip factor" needed to calculate the synchrotron oscillation frequency.

In a truly uniform, weak-focusing, electric ring the off-momentum closed orbits are true circles with radius r, in which case Eq. (8) provides an analytic formula valid for all amplitudes. For our purposes this is somewhat academic however, as explicit quadrupoles make the benchmark lattices slightly "separated-function". Deflections in the quadrupoles cause the off-momentum trajectories to be somewhat non-circular in the bends.

4.2 Dispersion of the Benchmark Lattices

Of the benchmark lattices, the closest to the ideal case is the `E_BM_Z.RF` lattice for which the quadrupoles are very weak. We have found however, after the quadrupoles have been adjusted to give identical tunes for the three benchmark cases, that the longitudinal behaviors of the three lattices are essentially identical. For example we will use Eq. (8) to estimate the dispersion for the `E_BM_M1.0` lattice.

In Eq. (8) the value $m = 0$ is singular; this corresponds to the fact that, for $m = 0$, γ^I is equal to γ_0, independent of r. Exploiting this independence, and neglecting a small m-dependent term that comes from treating the radial electric field as being independent of r, the dependence of γ (which, remember, is γ^O by definition) and r is

$$\mathcal{E}^O = m_p c^2 \gamma \approx m_p c^2 \gamma_0 + eE_0(r - r_0). \tag{9}$$

Differentiating with respect to r gives

$$d\mathcal{E}^O = eE_0 dr. \tag{10}$$

Using Eq. (2), this can be re-expressed as

$$dr = \frac{p_0 c/e}{E_0} \delta_{\text{UAL}}. \tag{11}$$

The UAL-units dispersion is therefore given by

$$r_{\text{co}}(\delta_{\text{UAL}}) = D_{\text{UAL}} \delta_{\text{UAL}}, \quad \text{where} \quad D_{\text{UAL}} = \frac{p_0 c/e}{E_0} = \frac{0.701}{10.48 \times 10^{-3}} = 66.9 \, \text{m}. \tag{12}$$

Figures 9 and 10 obtained by UAL/ETEAPOT tracking, agree very well with this estimate. Especially Figure 10, for which horizontal betatron motion has been largely eliminated, the straight line fit using Eq. (12) agrees perfectly with the tracking results.

4.3 Slip Factor and Synchrotron Tune

The revolution period of the central particle is given by

$$T_{\text{rev}}(\gamma_0) = \frac{2\pi r_0 + D_{\text{tot}}}{\beta_0 c}, \tag{13}$$

where $D_{\text{tot}} = 331.3274 - 2\pi \times 40 = 80.0 \, \text{m}$ is the accumulated straight section length. Neglecting the effect of the quadrupoles, for an off-momentum closed orbit, the revolution period is

$$T_{\text{rev}}(\gamma) = \frac{2\pi r}{\beta_0 c} + \frac{D_{\text{tot}}}{\beta^O c}. \tag{14}$$

The constancy of β within the bend region in the $m = 0$ case is exploited in the first term, but the actual β^O value has to be used in the second term. (Because D_{tot} is so short for the benchmark lattices, this term is small for the benchmark lattices. But for long straight sections, as in the FNAL option, time of flight through straight regions strongly influences the longitudinal motion.)

From $\beta^2 = 1 - 1/\gamma^2$ we have, evaluated at $\beta = \beta_0$, $d\beta = d\gamma/(\beta_0 \gamma_0^3)$. Using this in Eq. (9), and applying Eq. (12), the off-momentum, outside, velocity is

$$\beta^O \approx \beta_0 \left(1 + \frac{1}{\beta_0^2 \gamma_0^3} \frac{E_0}{m_p c^2/e} D_{\text{UAL}} \delta_{\text{UAL}}\right) = \beta_0 \left(1 + \frac{D_{\text{UAL}} \delta_{\text{UAL}}}{r_0 \gamma_0^2}.\right) \tag{15}$$

7

Substituting $r - r_0 \approx D_{\text{UAL}}\delta_{\text{UAL}}$ also into Eq. (14) yields

$$\frac{T_{\text{rev}}(\gamma) - T_{\text{rev}}(\gamma_0)}{T_{\text{rev}}(\gamma_0)} = \frac{1}{\mathcal{C}}\left(2\pi \mp \frac{1}{\gamma_0^2}\frac{D_{\text{tot}}}{r_0}\right)D_{\text{UAL}}\delta_{\text{UAL}}, \tag{16}$$

where $\mathcal{C}$ is the circumference of the design orbit. The $\mp$ factor in the second term allows for the fact that D_{UAL} can have either sign, while the phase slip in the straight section is necessarily negative. Edwards and Syphers[3] define the "slip factor" η_{RF} by

$$\frac{T_{\text{rev}}(\gamma + \Delta\gamma) - T_{\text{rev}}(\gamma_0)}{T_{\text{rev}}(\gamma_0)} = \frac{\eta_{\text{RF}}}{\beta_0^2}\frac{\Delta\gamma}{\gamma_0}, \tag{17}$$

and we obtain

$$\eta_{\text{RF}} = \beta_0\left(2\pi \mp \frac{1}{\gamma_0^2}\frac{D_{\text{tot}}}{r_0}\right)\frac{D_{\text{UAL}}}{\mathcal{C}} = -0.92. \tag{18}$$

As mentioned above, the negative sign is accounted for in the tracking simulation by shifting the RF phase appropriately to produce stable motion.

Edwards and Syphers give the synchrotron tune in terms of the slip factor:

$$Q_s = \sqrt{\frac{1}{2\pi}\frac{h_{\text{RF}}\eta_{\text{RF}}\cos(2\pi\text{lag})}{\beta_0^2\gamma_0}\frac{V_{\text{RF}}}{m_p c^2/e}} = 0.0061. \tag{19}$$

The $\eta_{\text{RF}}\cos(2\pi\text{lag})$ product needs to be positive for the synchrotron oscillations to be stable. The lag factor, which establishes the RF phase, is read in from the SXF lattice description file. (This is discussed further in a concluding section.)

5   Determination of Dispersion Function from Transfer Matrices

Orbit evolution from the origin at $s = 0$ to a general position s can be expressed by a transfer matrix $\mathbf{M}(s,0)$:

$$\begin{pmatrix} x(s) \\ x'(s) \\ \delta \end{pmatrix} = \begin{pmatrix} M_{11}(s,0) & M_{12}(s,0) & M_{13}(s,0) \\ M_{21}(s,0) & M_{22}(s,0) & M_{23}(s,0) \\ 0 & 0 & 1 \end{pmatrix}\begin{pmatrix} x(0) \\ x'(0) \\ \delta \end{pmatrix}. \tag{20}$$

Note that the third component is conserved except at RF cavities. Also some of th matrix elements depend on the definition of δ. After associating a transfer matrix to each of the elements in the ring, $\mathbf{M}(s,0)$ is found by "concatenating" (i.e. multiplying) these matrices.

For fully-relativistic magnetic lattices the third component δ is customarily referred to as $\delta p/p$, and this coordinate can be identified almost exactly with $\delta\gamma/\gamma$ or with fractional energy offset (from the design orbit). But for an only weakly-relativistic EDM lattice which, furthermore, has electric bending, it is necessary to be more careful. For now we leave the definition of δ open, planning to replace it by one or the other of the fractional offset coordinates introduced in the previous section. Of course the dispersion function $D_\delta(s)$ becomes definite only when δ is defined unambiguously.

The "off-momentum closed orbit" $x_{\text{c.o.}}(\delta, s)$ is defined to be the unique orbit which, for longitudinal phase space displacement δ, closes on itself after a complete turn around the ring. The dispersion is then defined, in linearized approximation, by

$$x_{\text{c.o.}}(\delta, s) = D_\delta(s)\,\delta. \tag{21}$$

Since the transfer matrix includes a description of the influence of energy offset, it can also be used to find the dispersion function $D_\delta(s)$. First the "fixed point" at the origin, $(D_\delta(0), D'_\delta(0))$ has to be found. If the lattice has mirror symmetry, which is true for the benchmark lattices, the origin can be chosen on the axis of symmetry, and $D(s)$ is also mirror-symmetric; in this case $D'(s)|_{s=0} = 0$.

Evolution once around the ring, starting from the origin, of an off-energy particle on the closed orbit corresponding to its energy is described by the "once-around" transfer matrix $\mathbf{M}$:

$$\begin{pmatrix} D(0)\,\delta \\ 0 \\ \delta \end{pmatrix} = \begin{pmatrix} M_{11} & M_{12} & M_{13} \\ M_{21} & M_{22} & M_{23} \\ 0 & 0 & 1 \end{pmatrix} \begin{pmatrix} D(0)\,\delta \\ 0 \\ \delta \end{pmatrix}. \tag{22}$$

This provides two formulas,

$$D(0) = \frac{M_{13}}{1 - M_{11}} = -\frac{M_{23}}{M_{21}}, \tag{23}$$

one of which can be used as a consistency check. Evolution around the ring of $D(s)$ and $D'(s)$ is then given by

$$\begin{pmatrix} D(s) \\ D'(s) \\ 1 \end{pmatrix} = \begin{pmatrix} M_{11}(s) & M_{12}(s) & M_{13}(s) \\ M_{21}(s) & M_{22}(s) & M_{23}(s) \\ 0 & 0 & 1 \end{pmatrix} \begin{pmatrix} D(0) \\ 0 \\ 1 \end{pmatrix}. \tag{24}$$

Spelled out explicitly,

$$D(s) = D(0)\,M_{11}(s) + M_{13}(s),$$
$$D'(s) = D(0)\,M_{21}(s) + M_{23}(s). \tag{25}$$

6 ETEAPOT Longitudinal Dynamics Plots

Longitudinal dynamics in lattice `BM_M1.0.RF` (having m=-1) is shown in Figure 3. The three benchmark lattices are compared in the similar plots of Figure **??**. For this comparison only the three innermost amplitudes are tracked. In these plots three particles start at the origin traveling in the forward direction, with fractional energy offsets δ_{UAL} = 0.000001, 0.000002, 0.000003. The three plots are essentially identical. We interpret this to mean that the quadrupoles adjacent to the bend elements, having been adjusted to restore the vertical tune to its standard value $Q_y = 0.2$, effectively cancel the focusing effect coming from non-zero field index m. In other words, as far as longitudinal dynamics is concerned, the three benchmark lattices are equivalent.

Fractional offset $\delta_{\mathrm{UAL}} \equiv \delta\mathcal{E}/(p_0 c)$ is plotted against turn number for a range of values of RF amplitude $\hat{V}_{\mathrm{RF}}$ in Figure 5. The corresponding longitudinal phase space plots are shown in Figure 6.
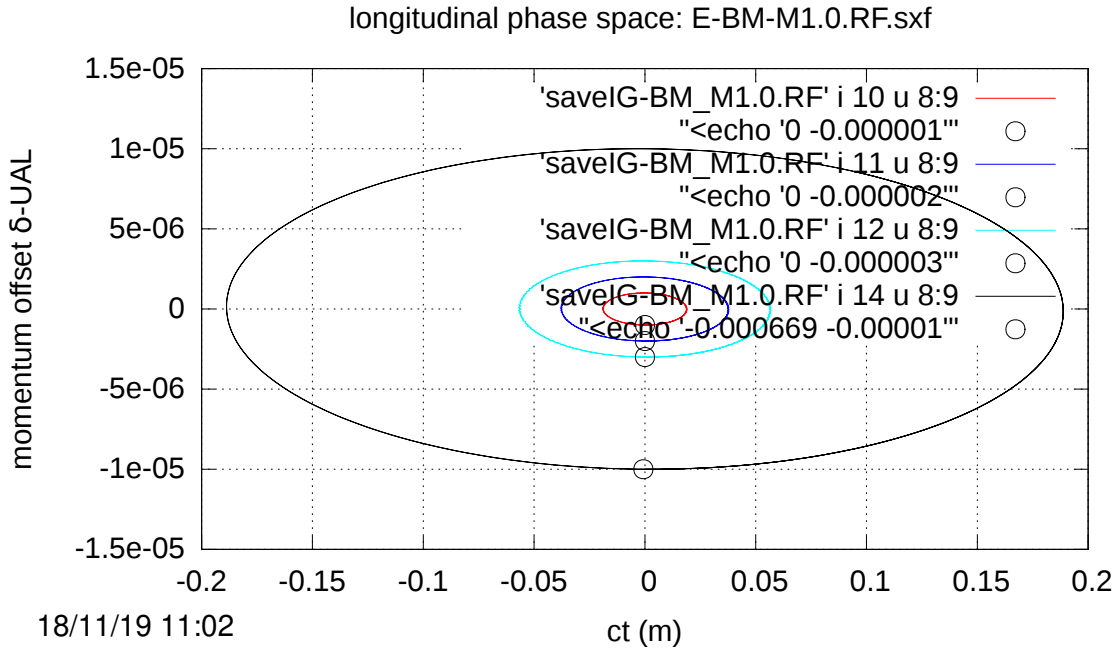
Figure 3: The longitudinal phase space for the `BM_M1.0.RF` lattice is extended to large amplitudes approaching the limit of stability for the given RF parameters. Fractional energy offsets are δ_{UAL} = 0.000001, 0.000002, 0.000003, 0.000010. Unlike the inner three contours, for the outermost contour the particle was launched with negligible initial betatron amplitude.

From Figures 5 and 6 data can be extracted to produce Figure 7 and Figure 8 which plot the synchrotron tune Q_s and the bunch length ℓ_B as functions of V_{RF}. Fitting functions are shown in the captions to the figures. The strict proportionality $Q_s \sim \sqrt{V_{\mathrm{RF}}}$ is consistent with Eqs. (19). Also consistent with theory, ℓ_B is proportional to $1/\sqrt{V_{\mathrm{RF}}}$.

Another aspect of longitudinal evolution is shown in Figure 9 for 500 turns for the smallest of the three amplitudes of the run shown in the middle (`E_BM_Z.RF.sxf`) case in Figure **??**. Figure 10 differs only in that initial conditions have been adjusted to eliminate betatron oscillations.

In Figure 11 only the initial horizontal slope is non-vanishing; $x' = -0.0004$. This is approximately the largest angle for which the particle will not be lost immediately on one of the electrodes which are situated at $x = \pm 0.015$ m. The trajectory clearly survives for the interval shown. Much longer runs will be shown below.

The two graphs of Figure 12 show the evolution of longitudinal position ct for small and large synchrotron oscillation amplitudes. Both motions are quite accurately sinusoidal.
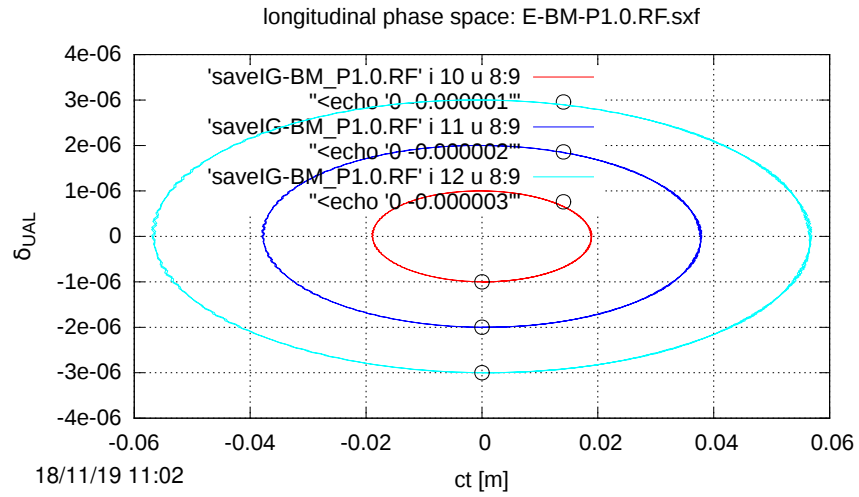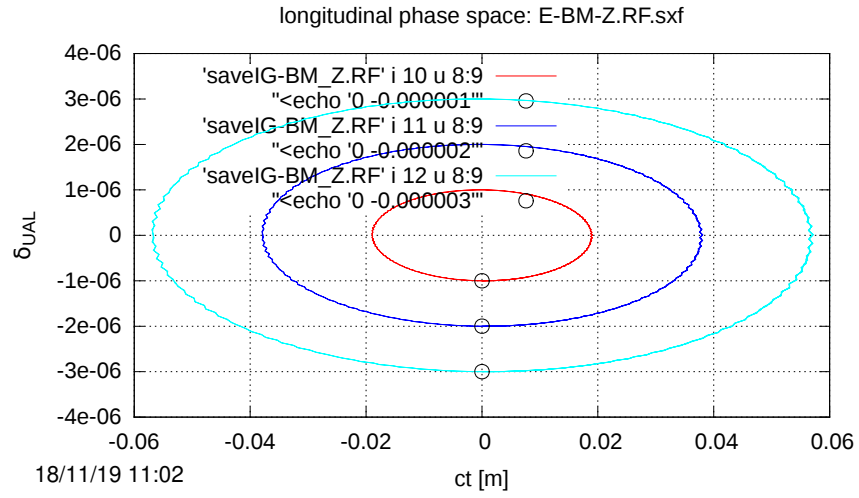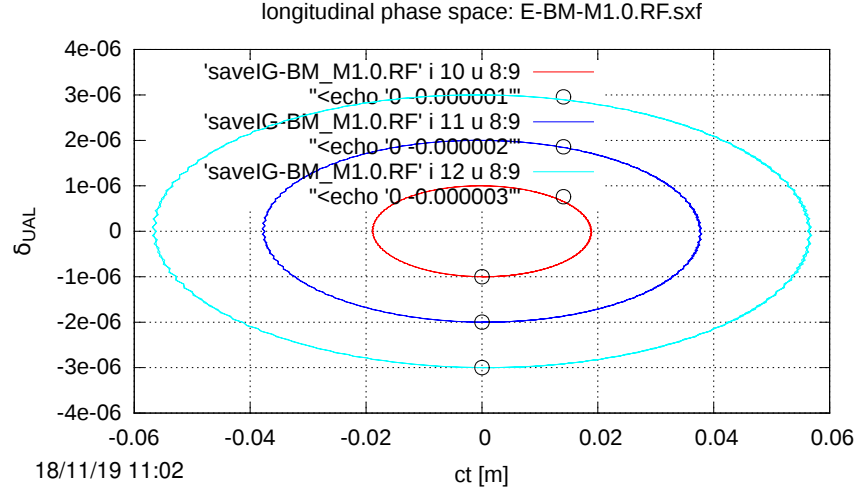
Figure 4: Longitudinal phase space plots for lattices (from top to bottom) BM_M1.0.RF, BM_Z.RF, and BM_P1p0.RF.
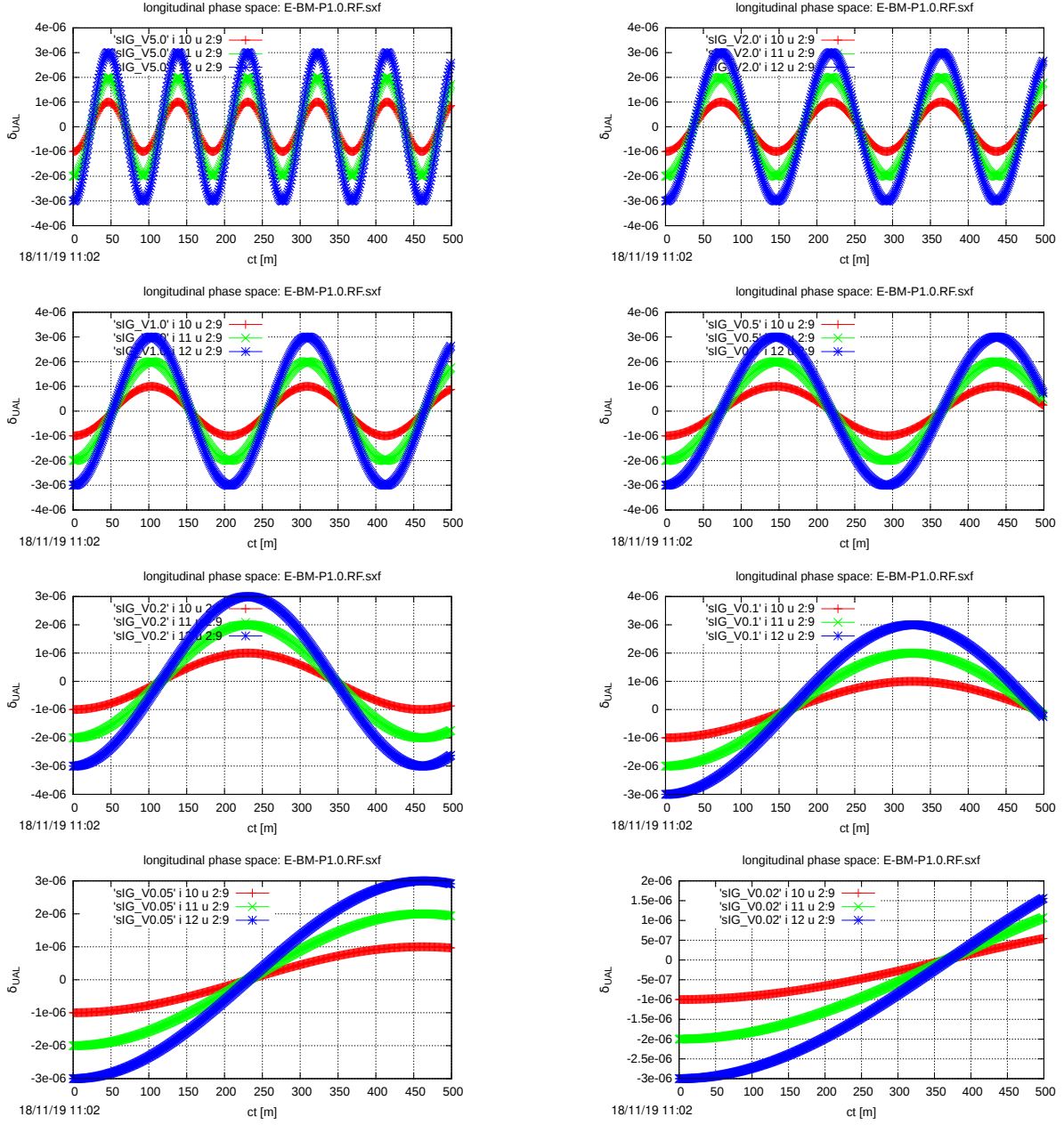
11

Figure 5: Fractional offset $\delta_{\mathrm{UAL}} \equiv \delta\mathcal{E}/(p_0 c)$ plotted against turn number for values of RF amplitude $\hat{V}_{\mathrm{RF}}$ 5.0, 2.0, 1.0, 0.5, 0.2, 0.1, 0.05, 0.02 [kV]—reading from left to right then top to bottom; lattice BM_M1.0.RF. Each of the plots shows three synchrotron oscillation amplitudes. Starting from the origin with vanishing slopes, the initial "momentum offsets" are δ_{UAL}=-0.000001,-0.000002, and -0.000003.
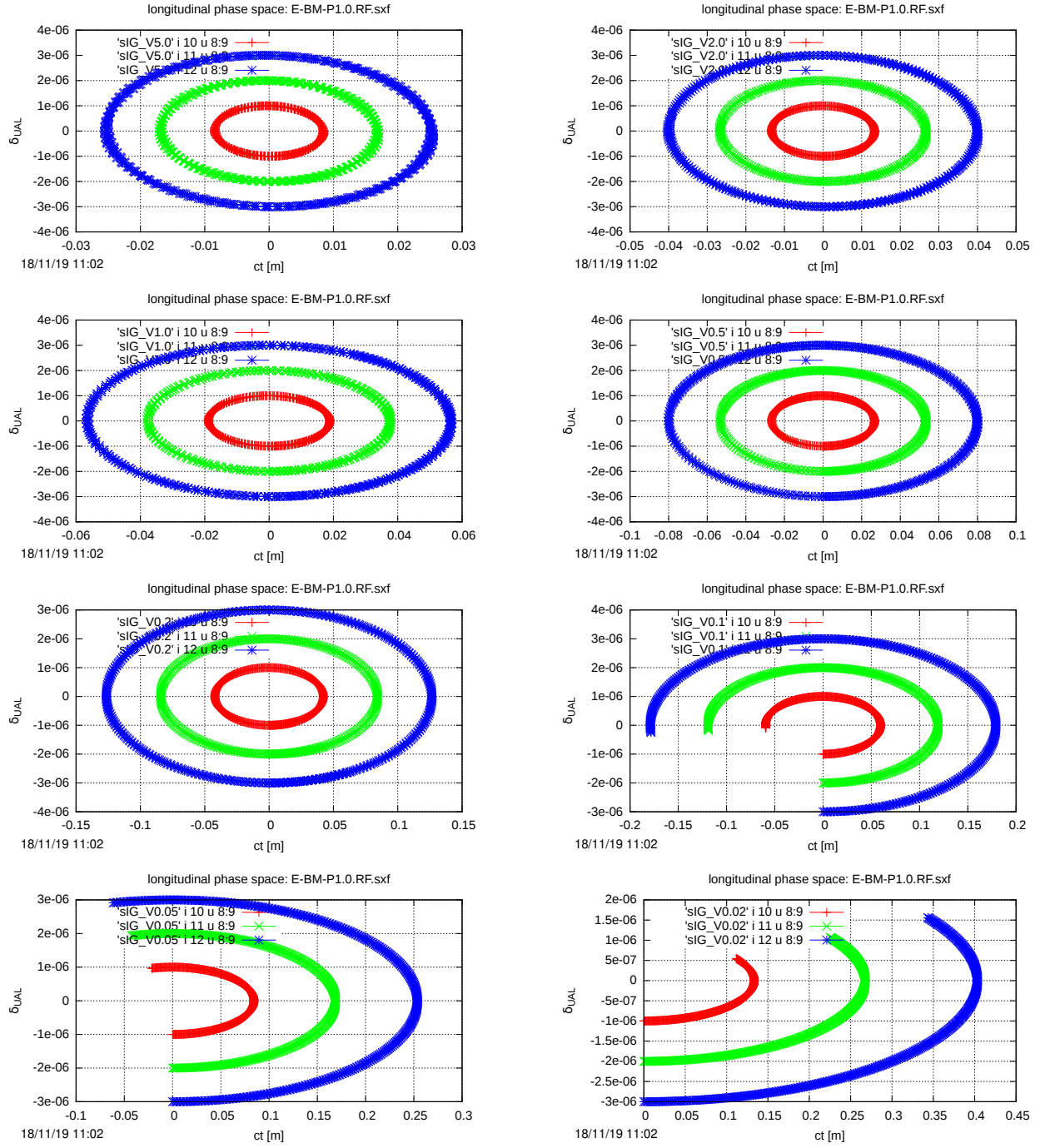
Figure 6: Longitudinal phase space plots for the same series of RF voltages, 5.0, 2.0, 1.0, 0.5, 0.2, 0.1, 0.05, 0.02 [kV] as in Figure 5. The horizontal axis is z in meters. The vertical axis is the fractional offset $\delta \mathcal{E}/(p_0 c)$.
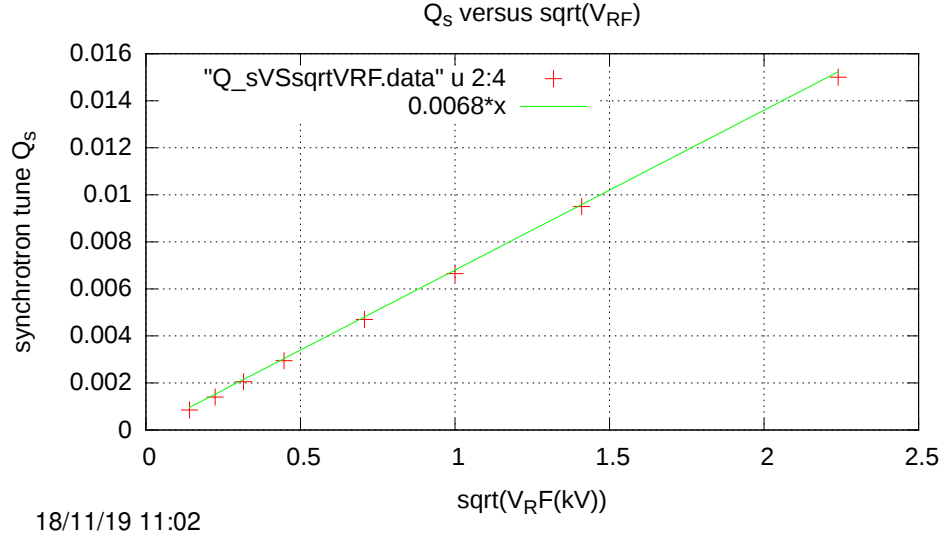
13

Figure 7: Plot of synchrotron tune Q_s (obtained by counting periods in plots like those in Figure 5) versus $\sqrt{V_{\mathrm{RF}}[kV]}$. The fit yields $Q_s = 0.00485\sqrt{V_{\mathrm{RF}}[kV]}$.
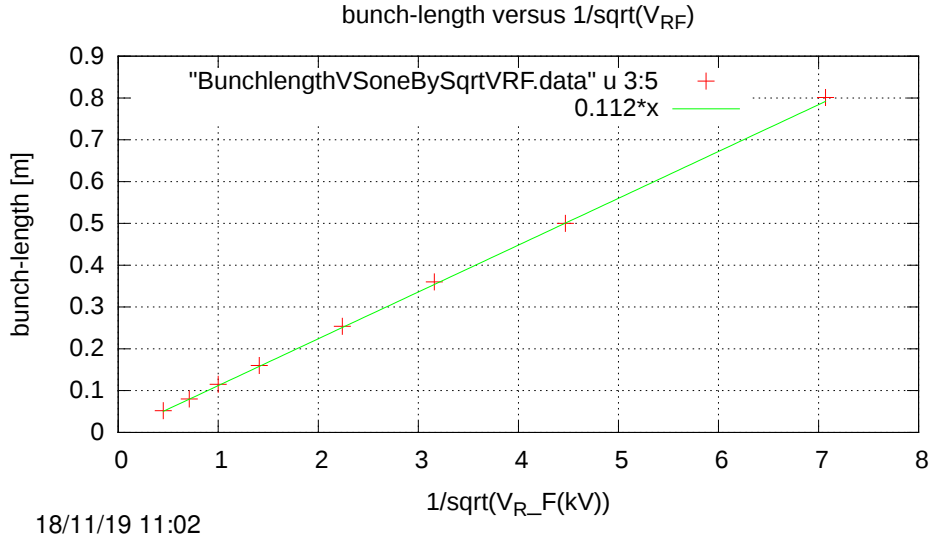

Figure 8: Plot of bunch length (extremes in plots like those in Figure 6 for δ_{UAL}=0.000003) versus $\sqrt{1/V_{\mathrm{RF}}[kV]}$. The fit yields $l_B = 0.112\,[\mathrm{m}]/\sqrt{V_{\mathrm{RF}}[\mathrm{kV}]}$.
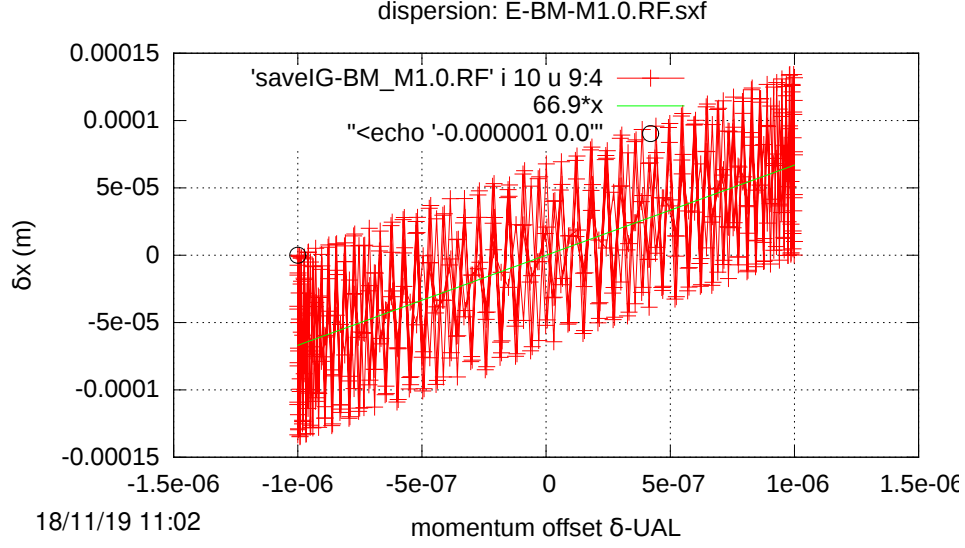
14

Figure 9: Starting at the black point, radial displacement x is plotted against fractional energy offset δ_{UAL}. The straight line corresponding to $D_{\mathrm{UAL}} = 66.9\,\mathrm{m}$, as given by Eq. (12), can be seen to give an excellent fit to the data. The scatter of points can be ascribed to horizontal betatron oscillations.
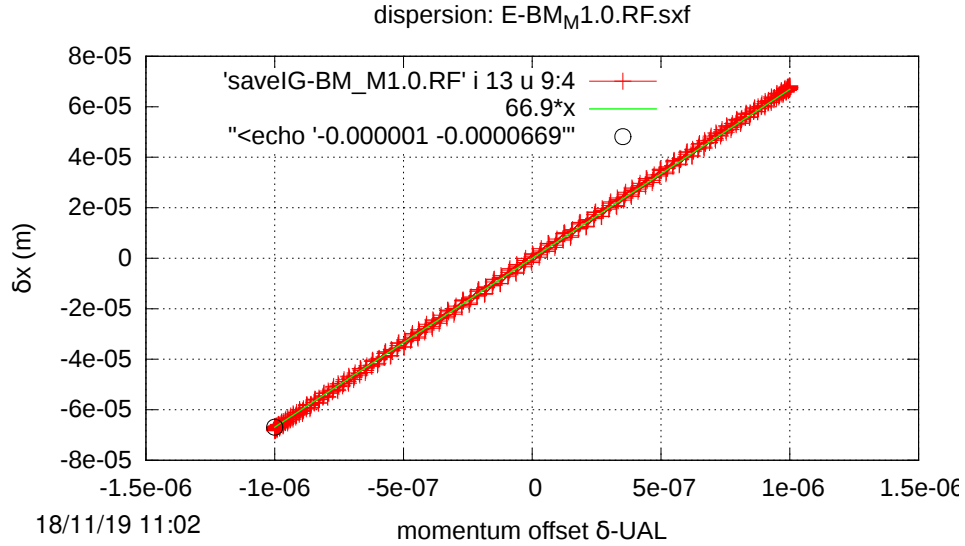

Figure 10: Same as Figure 9 except initial conditions have been assigned to minimize the initial horizontal betatron oscillation. So this is pure synchrotron oscillation, with radial position well fit by $x = 66.9[\mathrm{m}]\delta_{\mathrm{UAL}}$.
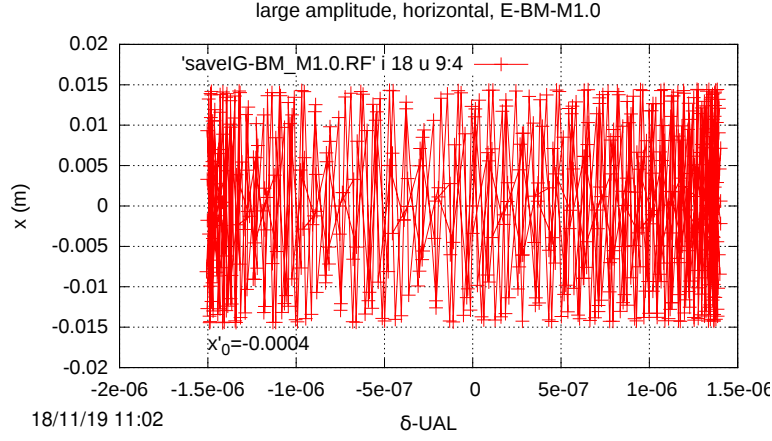
Figure 11: Large betatron amplitude, on-momentum, horizontal betatron motion in the E_BM_M1.0.RF.sxf lattice. Initial conditions are $(x = 0.0, x' = -0.0004, \delta_{\mathrm{UAL}} = 0)$. The graph with opposite initial slope $x' = 0.0004$ looks the same. With gap g being equal to $3\,\mathrm{cm}$, this particle is just inside the physical acceptance for the 500 turns shown.
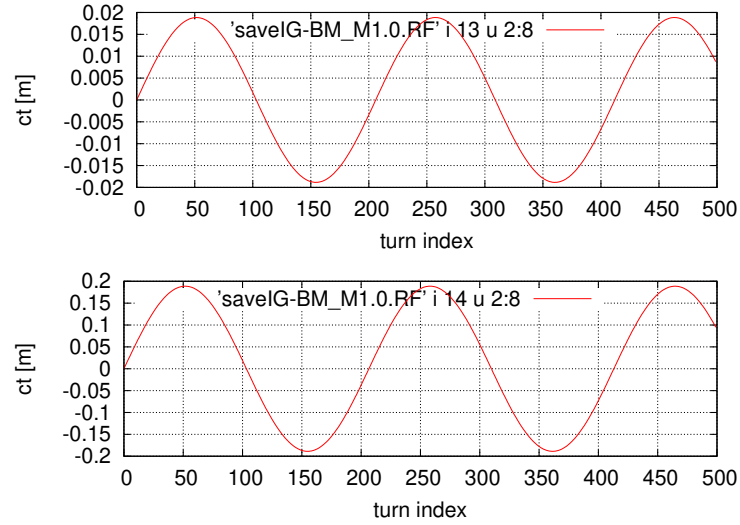

Figure 12: The upper graph plots longitudinal position ct vs. turn number for small amplitude synchroton oscillations. The tune Q_s is $2.45/500 = 0.0049$. The lower graph plots the same quantities but for ten times greater amplitude. The tune Q_s is $2.4/500 = 0.0048$.

16

Long term stability is investigated in Figure 13. Before the bug fix, for an intermediate case (third from the top), the beam blew up radially and fatally after tens of thousands of turns. After the bug fix the motion is stable at all investigated amplitudes.

The orbits were stable for one million turns in a weekend long run. Quantitatively, the exhibited growth, if interpreted as spurious, would correspond to a spurious growth lifetime of 3×10^6 turns.
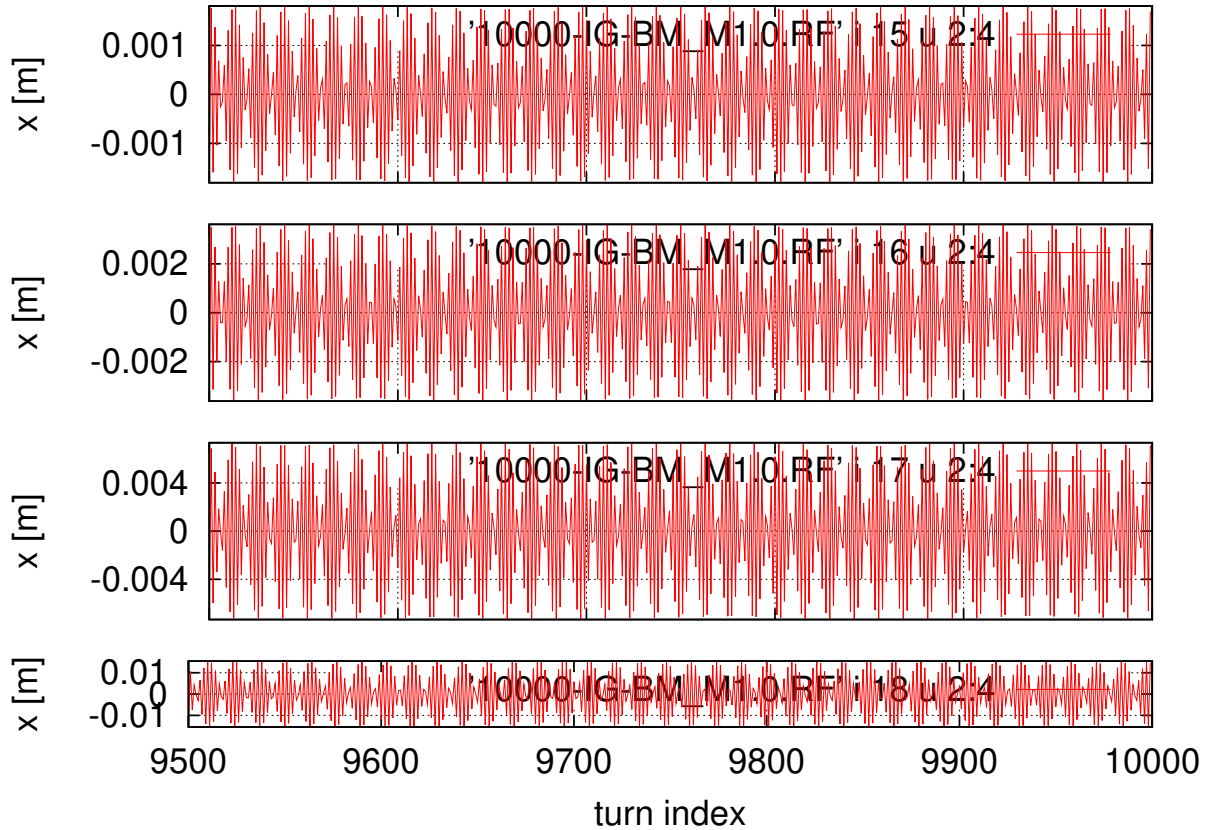

Figure 13: Tracking on-momentum particles with initial x' slopes of -0.00005, -0.0001, -0.0002, and -0.0004 for 10,000 turns in the E_BM_M1.0.RF.sxf lattice. Only the last 500 turns are shown. Even the largest amplitude case is stable indefinitely.

7 Summary

7.1 Comments and (Tentative) Conclusions

With a few significant exceptions, the various plots exhibit behaviour much like what one sees in magnetic lattices. Various numerical comparisons of momentum-dependent ETEAPOT tracking results with analytic calculations and with results from the linearized transfer matrix model are listed in Table 2. We consider the following points to be significant:

- We have found no significant differences in longitudinal dynamics among the three benchmark lattices (which have field index $m = -1, 0, 1$.) The discrete quadrupoles have been adjusted to give exactly the same vertical tunes and very nearly the same horizontal tunes. Apparently this constrains the longitudinal dynamics to be equivalent.

17

- There is essentially perfect agreement on the dispersion which is $D_{\text{UAL}} = 66.9\,\text{m}$. ($D_{dp/p} = \beta_0 D_{\text{UAL}} = 40.1\,\text{m}$.) Note, for example, Figure 10, which shows pure synchrotron oscillation with $x[m] = 66.9\,\delta_{\text{UAL}}$.

- ETEAPOT's determination of the small amplitude synchrotron tune is $Q_s = 0.0049$, which is significantly different from the "analytic" value $Q_s = 0.0061$. Noting that "analytic" and "correct" are not synonyms, clearly one or the other is wrong. Copied from the magnetic ring formalism, the analytic calculation assumes the absence of coupling between synchrotron an betatron oscillation, which is patently wrong. In other words, the analytic result is over-simplified. (The linearized transfer matrix model determination does not provide an independent check of longitudinal motion other than the value of lattice dispersion.)

- What makes the determination of synchrotron tune Q_s challenging is that it is hard to calculate the time of flight accurately. Apart from the fact that the fractional path length variations are miniscule, the change of velocity caused by change of potential has to be accounted for very accurately. Our calculation, based on analytic evaluation of the time of flight integral should, however be accurate and has been checked independently. We are now evaluating times of flight by two independent methods. Spot check comparisons of the two methods agree, typically to eight significant figures. (As it happens, before the bug fix, the error in the time of flight calculation was due to error in start and stop times rather than incorrect evaluation of the time of flight integral.)

- The ETEAPOT evaluation of spin precession in bend elements proceeds using formalism just like the time of flight formalism. The spin precession integrals are elementary and do not require either approximate or power series evaluation to be expressable in exact closed form.

- The phase space has not been adequately investigated to obtain an accurate horizontal admittance value. A rough estimate derived from just the angular acceptance comes from $|x'_{\text{max}}| \approx \sqrt{\epsilon_{\text{admittance}}/\beta_x}$ or

$$\epsilon_{\text{admittance}} \approx \beta_x {x'_{\text{max}}}^2 = 36 \times 0.0004^2 = 5.8 \times 10^{-6}\,\text{m}. \tag{26}$$

This is substantially larger than the value $10^{-6}\,\text{m}$ used in some preliminary parameter estimations.

- The results of the previous version of this report strongly suggested that the magnitude of the lattice dispersion in the pEDM benchmark lattices being considered was unacceptably large. This may still be true, but that conclusion can no longer be based on the ETEAPOT tracking, as it was, for example, in our separate report[6].

- That report proposed a minimized-dispersion, combined function lattice that is strong-focusing horizontally and (as favored for the EDM measurement) weak-focusing vertically. Of all the lattices that have been contemplated for the proton EDM experiment, that alternating gradient lattice most nearly resembled the very first all-electric lattice, which was built at BNL for the very first alternating gradient proton accelerator[7].

- In that report, both the experience with ELISA and the discouraging ETEAPOT tracking argued that the EDM ring dispersion had to be reduced. The ELISA experience construes to be worrisome, but the (quite limited) ETEAPOT tracking only supports what has always been known—the injected momentum spread has to be very small. But long spin coherence time also requires tiny momentum spread, so these two requirements are, at least, compatible.

- We have therefore reverted to the opinion that it is an open question as to whether or not alternating gradient focusing is really needed for the proton EDM experiment.

References

[1] J.D. Talman and R.M. Talman, *UAL/ETEAPOT Results (Augmented) for Proton EDM Benchmark Lattices,* BNL internal report, April 29, 2012

[2] J.D. Talman and R.M. Talman, *UAL/ETEAPOT Proton EDM Benchmark Comparisons II: Transfer Matrices and Twiss Functions,* BNL internal report, August 30, 2012

[3] D. Edwards and M. Syphers, *Longitudinal Motion,* p. 53 in *Handbook of Accelerator Physics and Engineering,* editors, A. Chao and M. Tigner, World Scientific, 2002

[4] N. Malitsky, J. Talman, and R. Talman, *Appendix UALcode: Development of the UAL/ETEAPOT Code for the Proton EDM Experiment,* UAL/ETEAPOT documentation (frequently revised), August, 2012

[5] Storage Ring EDM Collaboration, *A Proposal to Measure the Proton Electric Dipole Moment with 10^{-29} e-cm Sensitivity,* especially Appendix 1. October, 2011

[6] R. Talman, *Reduced Dispersion Proton EDM Storage Ring Lattices,* Internal Report, 12 December, 2012

[7] M. Plotkin, *The Brookhaven Electron Analog, 1953-1957,* Brookhaven Internal Report, BNL-45058, 1991

[8] E. Forest, *Beam Dynamics, A New Attitude and Framework,* Harwood Academic Publishers, 1998. See especially Section 12.2.3,